ATLAS NOTE

Design, Construction and Installation of the ATLAS Hadronic Barrel Scintillator-Tile Calorimeter

The Tile Calorimeter Subsystem of the ATLAS Collaboration

J. Abdallah[1], P. Adragna[2], C. Alexa[3], R. Alves[4], P. Amaral[5],[6], A. Ananiev[7], K. Anderson[8], X. Andresen[5],[6], A. Antonaki[9], V. Batusov[10], P. Bednar[11], E. Bergeaas[12], C. Biscarat[13], O. Blanch[14], G. Blanchot[14], C. Bohm[12], V. Boldea[3], F. Bosi[2], M. Bosman[14], C. Bromberg[15], J. Budagov[10], D. Calvet[13], C. Cardeira[7], T. Carli[5], J. Carvalho[4], M. Cascella[2], M.V. Castillo[1], J. Costello[1], M. Cavalli-Sforza[14], V. Cavasinni[2], A.S. Cerqueira[16], C. Clement[5],[12], M. Cobal[5], F. Cogswell[17], S. Constantinescu[3], D. Costanzo[2], P. Da Silva[16], M. David[6] T. Davidek[18],[5], J. Dawson[19], K. De[20], T. Del Prete[2], B. Di Girolamo[5], S. Dita[3], J. Dolejsi[18], Z. Dolezal[18], A. Dotti[2], R. Downing[17], G. Drake[19], I. Efthymiopoulos[5], D. Errede[17], S. Errede[17], A. Farbin[8],[5], D. Fassouliotis[9], E. Feng[8], A. Fenyuk[21], C. Ferdi[13], B.C. Ferreira[16], A. Ferrer[1], V. Flaminio[2], J. Flix[14], P. Francavilla[2], E. Fullana[1], V. Garde[13], K. Gellerstedt[12], V. Giakoumopoulou[9], V. Giangiobbe[2], O. Gildemeister[5], V. Gilewsky[22], N. Giokaris[9], N. Gollub[5], A. Gomes[6], V. Gonzalez[1], J. Gouveia[7], P. Grenier[5],[13], P. Gris[13], V. Guarino[19], C. Guicheney[13], A. Gupta[8], H. Hakobyan[23], M. Haney[17], S. Hellman[12], A. Henriques[5], E. Higon[1], N. Hill[19], S. Holmgren[12], I. Hruska[24], M. Hurwitz[8], J. Huston[15], I. Jen-La Plante[8], K. Jon-And[12], T. Junk[17], A. Karyukhin[21], J. Khubua[25],[10], J. Klereborn[12], S. Kopikov[21], I. Korolkov[14], P. Krivkova[18], Y. Kulchitsky[22],[10], Yu. Kurochkin[22], P. Kuzhir[26], V. Lapin[21], T. Le Compte[19], R. Lefevre[13], R. Leitner[18], J. Li[20], M. Liablin[10], M. Lokajicek[24], Y. Lomakin[10], P. Lourtie[7], L. Lovas[11], A. Lupi[2], C. Maidantchik[16], A. Maio[6], S. Maliukov[10], A. Manousakis[9], C. Marques[6], F. Marroquim[16], F. Martin[5],[13], E. Mazzoni[2], F. Merritt[8], A. Miagkov[21], R. Miller[15], I. Minashvili[10], L. Miralles[14], G. Montarou[13], S. Nemecek[24], M. Nessi[5], I. Nikitine[21], L. Nodulman[19], O. Norniella[14], A. Onofre[27], M. Oreglia[8], B. Palan[24], D. Pallin[13], D. Pantea[3], A. Pereira[4], J. Pilcher[8], J. Pina[6], J. Pinhão[4], E. Pod[8], F. Podlyski[13], X. Portell[14], J. Poveda[1], L. Pribyl[24], L.E. Price[19], J. Proudfoot[19], M. Ramalho[7], M. Ramstedt[12], L. Raposeiro[7], J. Reis[7], R. Richards[15], C. Roda[2], V. Romanov[10], P. Rosnet[13], P. Roy[13], A. Ruiz[1], V. Rumiantsau[26], N. Russakovich[10], J. Sa da Costa[7], O. Salto[14], B. Salvachua[1], E. Sanchis[1], H. Sanders[8], C. Santoni[13], J. Santos[6], J.G. Saraiva[6], F. Sarri[2], L.-P. Says[13],

[1] IFIC, Centro Mixto Universidad de Valencia-CSIC, E46100 Burjassot, Valencia, Spain

[2] Pisa University and INFN, Pisa, Italy

[3] Institute of Atomic Physics, Bucharest, Romania

[4] LIP and FCTUC Univ. of Coimbra, Portugal

[5] CERN, Geneva, Switzerland

[6] LIP and FCUL Univ. of Lisbon, Portugal

[7] LIP and IDMEC-IST, Lisbon, Portugal

[8] University of Chicago, Chicago, Illinois, USA

[9] University of Athens, Athens, Greece

[10] JINR, Dubna, Russia

[11] Comenius University, Bratislava, Slovakia

[12] Stockholm University, Stockholm, Sweden

[13] LPC Clermont–Ferrand, Université Blaise Pascal, Clermont-Ferrand, France

[14] Institut de Fisica d'Altes Energies, Universitat Autònoma de Barcelona, Barcelona, Spain

[15] Michigan State University, East Lansing, Michigan, USA

[16] COPPE/EE/UFRJ, Rio de Janeiro, Brazil

[17] University of Illinois, Urbana–Champaign, Illinois, USA

[18] Charles University in Prague, Prague, Czech Republic

[19] Argonne National Laboratory, Argonne, Illinois, USA

[20] University of Texas at Arlington, Arlington, Texas, USA

[21] Institute for High Energy Physics, Protvino, Russia

[22] Institute of Physics, National Academy of Sciences, Minsk, Belarus

[23] Yerevan Physics Institute, Yerevan, Armenia

[24] Institute of Physics, Academy of Sciences of the Czech Republic, Prague, Czech Republic

[25] HEPI, Tbilisi State University, Tbilisi, Georgia

[26] National Centre of Particles and High Energy Physics, Minsk, Belarus

[27] LIP and Univ. Católica Figueira da Foz, Portugal

2

G. Schlager[5], J. Schlereth[19], J.M. Seixas[16], B. Selldèn[12], N. Shalanda[21], P. Shevtsov[26], M. Shochet[8], J. Silva[6], V. Simaitis[17], M. Simonyan[23], A. Sissakian[10], J. Sjoelin[12], C. Solans[1], A. Solodkov[21], O. Solovianov[21], M. Sosebee[20], F. Spano[5],[2], P. Speckmeyer[5], R. Stanek[19], E. Starchenko[21], P. Starovoitov[26], M. Suk[18], I. Sykora[11], F. Tang[8], P. Tas[18], R. Teuscher[8], S. Tokar[11], N. Topilin[10], J. Torres[1], D. Underwood[19], G. Usai[2], A. Valero[1], S. Valkar[18], J.A. Valls[1], A. Vartapetian[20], F. Vazeille[13], C. Vellidis[9], F. Ventura[7], I. Vichou[17], I. Vivarelli[2], M. Volpi[14], A. White[20], A. Zaitsev[21], A. Zenin[21], T. Zenis[11], Z. Zenonos[2], S. Zenz[8], B. Zilka[11]

Abstract

This paper summarises the design, mechanical construction and installation of the scintillator/tile hadronic calorimeter for the ATLAS experiment at the Large Hadron Collider in CERN, Switzerland. The mechanical construction of the tile calorimeter occurred over a period of about 10 years beginning in 1995 with the completion of the technical design report, used as the basis for construction, and ending in 2005 with the installation of the final module in the ATLAs cavern. During this period approximately 2600 metric tons steel was transformed into a laminated structure to form the absorber of the sampling calorimeter. Following instrumentation and testing, which is described elsewhere, the modules were installed in the ATLAS cavern with a remarkable, and possibly unprecedented, accuracy for a structure of this size. The assembly work was distributed throughout the collaboration, and itself was a logistical challenge of no small magnitude. This project was a truly global effort and has culiminated in the installation of this calorimeter in the ATLAS cavern, where it is now being commissioned for first physics data-taking.
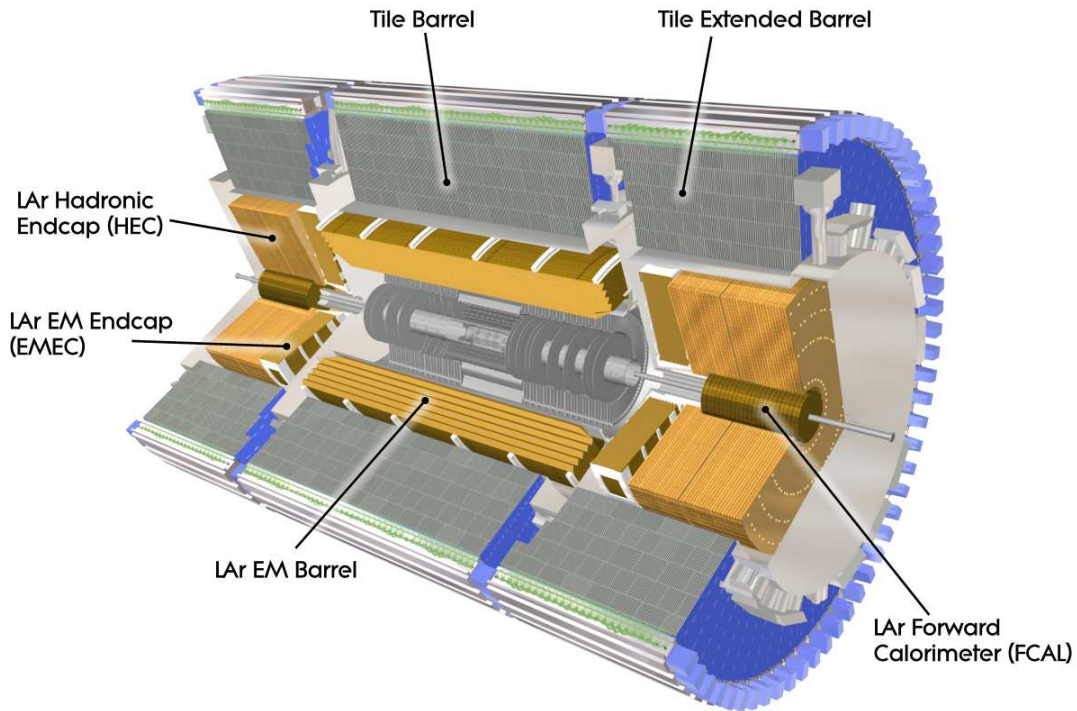
1 Introduction

Figure 1: The calorimeter system in the ATLAS experiment at the Large Hadron Collider.

Figure 1 shows the layout of the calorimeter system of ATLAS [1]. The scintillator-tile hadronic calorimeter (TileCal) [2] for ATLAS is physically the largest component in this system with the function of extending the depth of calorimetry to wholly contain hadronic showers from particles emitted in pp collisions at the interaction point. It is a sampling calorimeter using steel as the absorber structure and scintillator as the active medium. The scintillator is located in pockets in the steel structure and the scintillation light is read out using wavelength-shifting fibers which couple the it to photomultiplier tubes which are located inside the outer support girders of the calorimeter structure. In addition to its role as a detector for high energy particles, the tile calorimeter provides the direct support of the liquid argon electromagnetic calorimeter in the barrel region, and the liquid argon electromagnetic and hadronic calorimeters in the endcap region. Through these, it indirectly supports the inner tracking system and beam pipe. The steel absorber, and in particular the support girders, provide the flux return for the solenoidal field from the central solenoid. Finally, the end surfaces of the barrel calorimeter are used to mount services, power supplies and readout crates for the inner tracking systems and the liquid argon barrel electromagnetic calorimeter.

2 Design

The tile calorimeter is constructed in 3 sections, one central barrel and two extended barrels, each comprising 64 units (termed modules), which are stacked on each other to form each cylinder (figures 1, 2). A Barrel module weighs 20020 kg and an Extended Barrel module weighs (9600 kg) for a total weight for the entire calorimeter of approximately 2600 metric tons. The mechanical structure has a nominal

outer diameter of 4230 mm and an inner diameter of 2288 mm. A barrel (extended barrel) module has a length of 5640 mm ($2900\mu^+\mu^-$). The calorimeter itself is self-supporting and rests simply on support saddles placed in the lower regions of the structure as discussed below. The instrumented region of the calorimeter has a radial length of 1.64 m, and contributes 7.4 hadronic interaction lengths for particles emitted at 90 degrees to the interaction point.
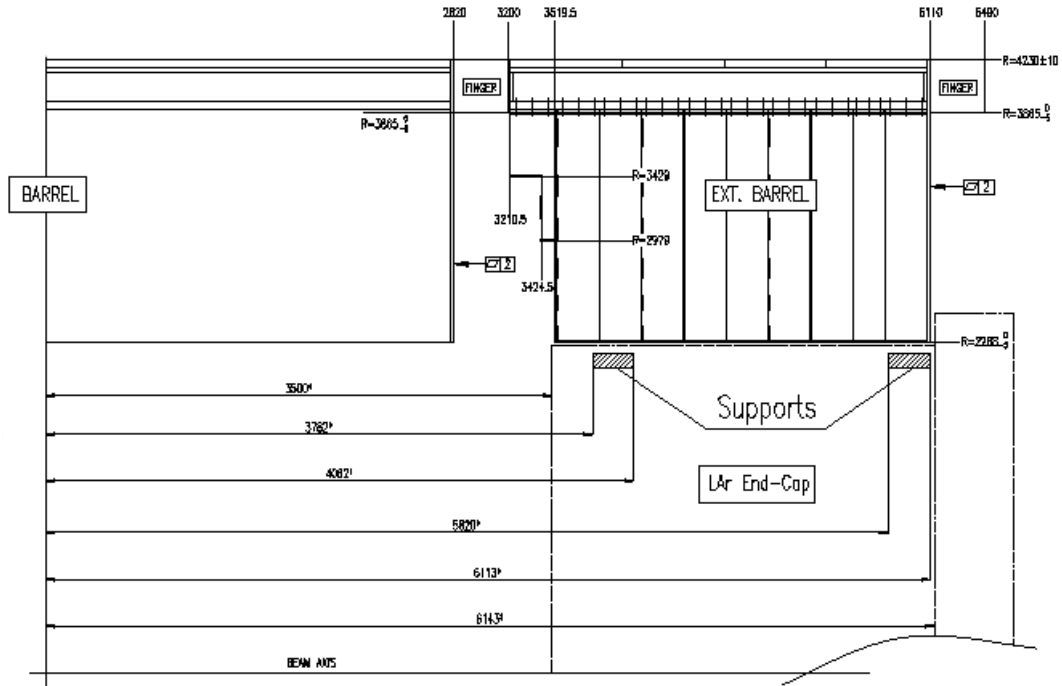

Figure 2: Design cross section along beam line of one half of the tile calorimeter. The structure is symmetrical about z=0. Note that the gap in z between barrel and extended barrel cylinders is adjustable, within some limits, and in the final installation is about 3 mm, with 3 fingers touching the extended barrel.

A key design constraint is to have a gap between modules. The fabrication and assembly tolerances provide for a design gap of 1.5 mm, thereby achieving the best fiducial coverage attained by any such stacked structure. To achieve this, the design contains a significant level of integration between the absorber mechanical structure, the active medium and its optical readout, and the electronics readout of the scintillation light by photomultipliers. In addition, the absorber structure is formed using steel laminations, and has the unique feature that the steel plates run radially outward from the beam axis. This is the feature of the mechanical design which allows the fiducial acceptance of this calorimeter to be as great as possible. We present the key characteristics of the calorimeter design below. Further details can be found in reference [2].

A schematic of the calorimeter structure is shown in figure 3. The structure is a glued and welded steel lamination of full-length plates (master plates) interspersed along their length by short plates (spacer plates) to form pockets in which the active medium, scintillator tiles, are inserted. The spacer plates are set back from the edge of the master plate outer envelope by approximately 1.5 mm to provide a slot in which the readout fibers will be inserted. The wrapped scintillator tiles are inserted into the slots and are read out by wavelength shifting fibers which are inserted in channels located between each of the pairs of full-length plates as indicated in figure 3. As a result, no additional absorber volume is compromised to acomodate the fiber readout and in addition the fibers themselves are protected from mechanical damage by being enclosed on three sides by the steel structure. A plastic channel is used to contain the fibers and provide a cost-effective approach for what would otherwise have been a labor intensive operation.

6
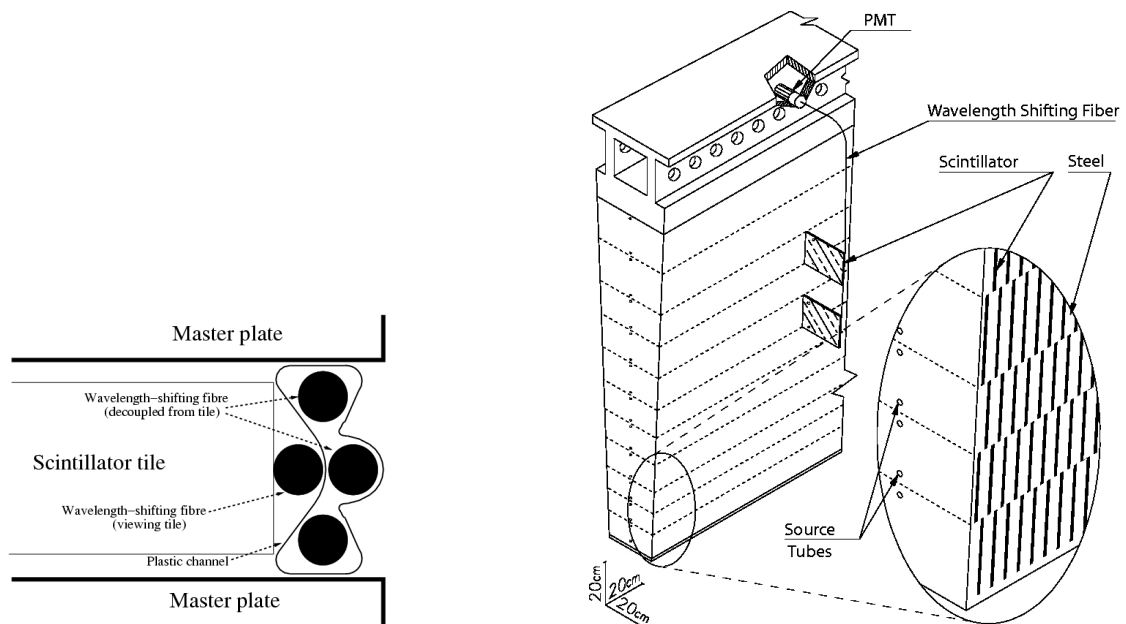
Figure 3: A schematic of the integration between the module absorber structure and the optical components. The view is radial, inwards toward the interaction point and illustrates the integration of the absorber with the scintillator and fibre readoure components (left). A schematic showing the sampling structure of the tile calorimeter and integration of scintillator tiles and readout fibers with the absorber structure running in radial lines from the interaction point (right).

Figure 4: The principal absorber is formed using 5mm thick steel plates, the so-called master plates.

The full-length plate, shown in figure 4, is the principal component of the calorimeter absorber structure. It is fabricated to high precision by die stamping. The slots at either end as well as the overall envelope of the plate are critical elements of the overall module envelope. In addition, the plate has 22 precisely located holes through which the tubes containing the calibration source mus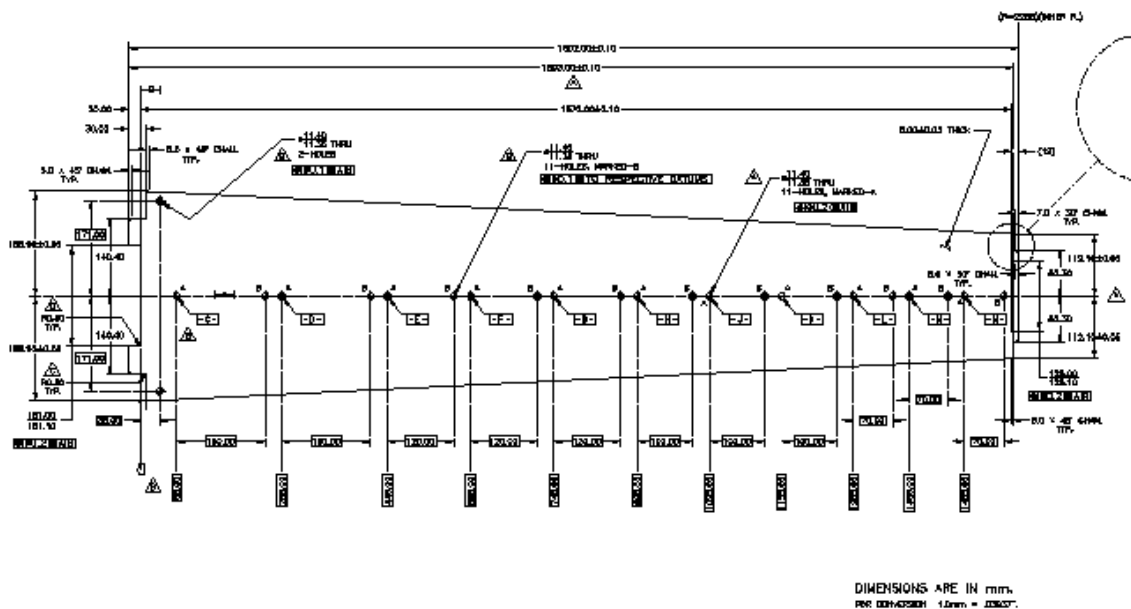t be inserted along the entire length of the structure. These holes have a diameter of 11.4 mm and sized to to match the pins used to mechanically fasten the spacer plates to master plates with the calibration tubes, which have an outer diameter of 8 mm Finally, the spacer plates are also dimensioned to high precision and are mechanically fastened to the master plate in order to realise the channel in which the readout fibers run and in particular to control the air gap between the fibres and the scintillator tiles.

This basic mechanical structure is formed into a series of subunits, termed submodules, which are bolted together along the length of a support girder to form each of the 192 modules. Each standard submodule has a length along the girder of 293.2 mm and weighs 865 kg. 8 standard submodules and two customized submodules are used to construct an extended barrel module, while 18 standard submodules and one customized submodule are used to construct a barrel module.

The outer structural support of the module is the girder. This is a precision, machined steel structure whose key role in the design is to provide the means to meet the envelope specification of the module in the alignment of submodules and in the definition of the outer radius bearing surface. In addition to providing the outer bearing surface, the support girder provides the magnetic flux return for the central solenoid and also houses the photomultipliers and front-end readout electronics for the calorimeter. The bearing surface and flux return are simple engineering issues. However the use of this structure to contain the readout electronics resulted in a unique and elegant solution to the conflicting constraints of high precision in the alignment of the photomultipliers to the wavelength-shifting fibers, while providing periodic access to the electronics for maintenance. The solution adopted is to locate the photomultipliers and readout electronics in drawers which can be extracted when necessary from the end of the girder (figure 5). The key mechanical elements in this interface are the girder rings, which are installed during
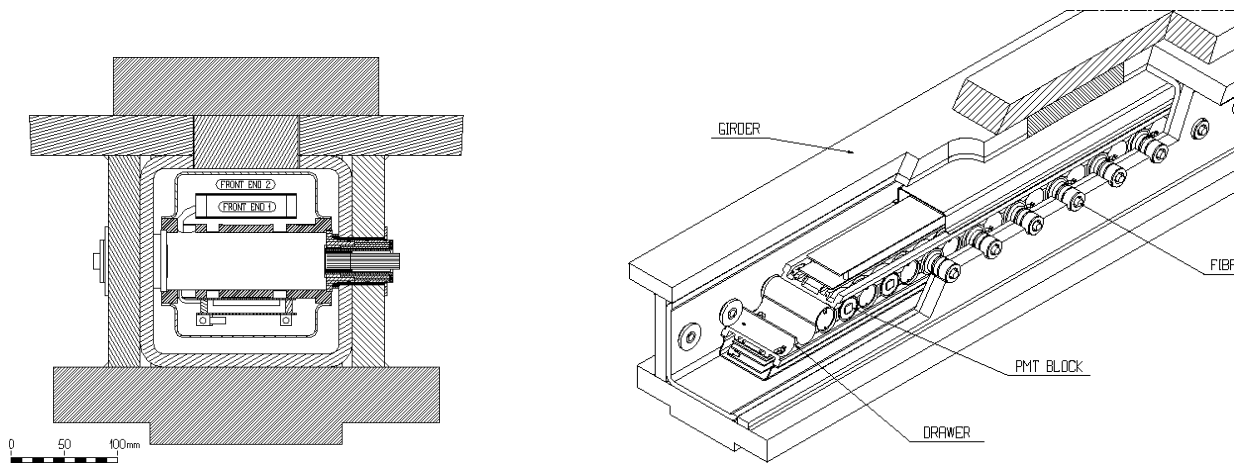
Figure 5: The cross section of the drawer inside the module support girder, and an example of the girder ring to drawer interface on the left hand side of the drawer and an example of the fiber bundle insertion into the girder ring on the right hand side of the drawer (left). A schematic of the electronics drawer inside the girder volume showing the rolling interface required for extraction and servicing of the calorimeter readout electronics (right).

module construction. The drawer rolls on these rings which are glued with high precision into the girder plates to control both the position along the length of the girder as well as the distance between the internal surface of the ring and that of the drawer. The typical precision is 0.3 mm along the length of the

girder and 0.1 mm between the light-mixer in front of the photomultiplier window and the wavelength-shifting fiber bundle.
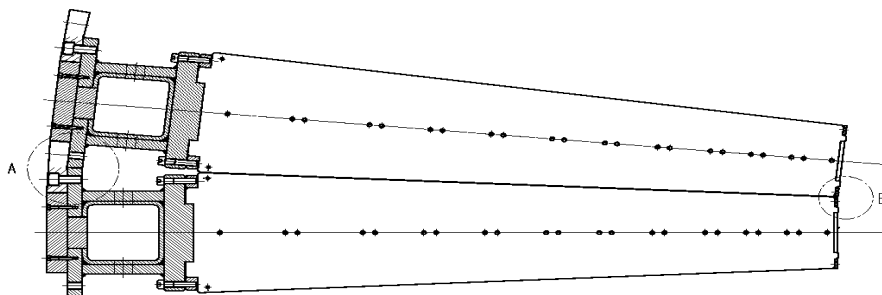

Figure 6: The gap between calorimeter modules showing the bearing locations at the inner and outer radii, thereby allowing the readout fibers to pass into the girder volume for coupling to the readout photomultiplier tubes. The circled sections indicate the load bearing locations at the inner radius of the modules and at the outer radius of the girder. Also shown is the bolted connecting plate.

The module-to-module radial interface in the cylinder assembly is shown in figure 6. The bearing points are at the inner radius and at the outermost edge of the support girder. In the initial design, the shim surface at the inner radius was conceived to be on 5 mm wide straps which were welded to the submodule for this purpose. More complete engineering calculations showed that this width of shim surface would be inadequate in the region of the endcap cryostat supports. In this region the shim surface required it to be on the master plate edges themselves and it was decided to use a common solution for the entire calorimeter. Adjustments in the thickness of these shims control the gap between modules and were later used during cylinder assembly to control the overall cylindrical geometry of the calorimeter. It should be noted that the girder width at the interface to the submodule matches the channel in which the fibers are routed so that there is a straight run for the fibers into the outer cavity of the girder.

The low voltage power supplies, cooling and readout cables enter the drawer at the end of the girder. These are all contained in extensions of the girder (called fingers) which provide shielding from the return magnetic field as well as physical protection for cables and connectors. The fingers can be seen in figure 2; there are two fingers on barrel modules and one finger for each extended barrel module. A typical finger with the services exposed is shown in figure 7 (additional plates are inserted to provide additional magnetic shielding before the finger is closed by a steel plate.) In the regions of the barrel cryostat supports, short fingers are required.

The region between the barrel and extended barrel calorimeters is a 3-dimensional jigsaw puzzle as the objec-

Figure 7: The inside of a finger with the services exposed.

tive in this region is to fit all services to the inner detector systems while minimizing the width of the gap between the two calorimeters. This is shown in figure 8, which shows the readout towers of the calorimeter pointing back to the interaction point. The projective geometry of the readout cells in the extended barrel calorimeter is relatively insensitive to the precise location of the calorimeter along the beam line and the the gap between the barrel and extended barrel calorimeters can be increased to accommodate changes in requirements for services (within the constraints of the cavern volume). Figure 8 also shows the scintillators which are placed in this region to provide signals to correct for energy loss in

9

the material of these services and structural supports .
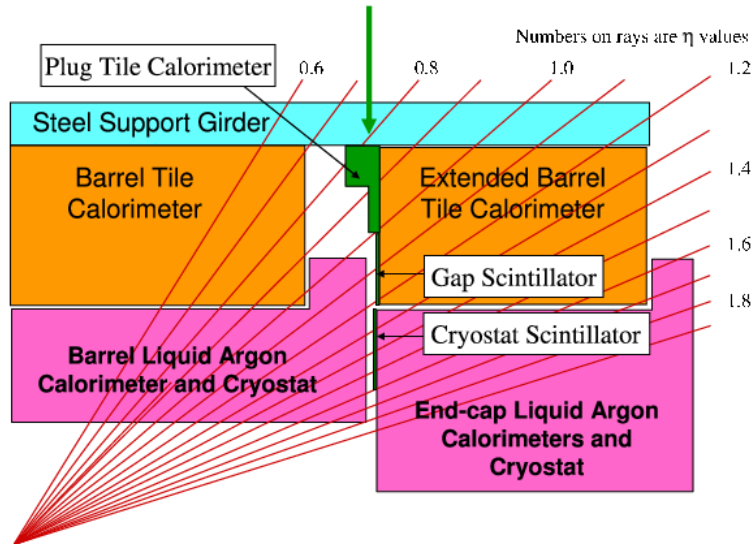

Intermediate Tile Calorimeter Concept

Figure 8: A cut through the calorimeter system at the interface between barrel and extended barrel calorimeter. Note that the support girder is in fact not physically continuous but comprises the separate girders for the barrel and extended barrel calorimeters, the fingers on the barrel and steel shims which are bolted to them. The picture is symmetrical about z=0.

There are a number of locations in the barrel and extended barrel where modules require modification to provide space for readout crates and services for the liquid argon calorimeters and the inner detector. In these regions the ITC submodule is reduced in size to provide additional space in the gap, as shown in figure 9, which illustrates the geometry for two of the three different types of customized ITC submodules. The third type is simply the steel endplate and has a single layer of

Figure 9: Layout of special ITC submodules.

scintillator over its surface. The locations of these modules around the cylinder are shown in figure 10 More details may be found in [2] [7].

The fundamental support of the calorimeter comes from saddles distributed along the length of the cylinders to transfer the load to the main ATLAS rails (figure 11). There are four such pairs of saddles along the length of the barrel cylinder and two along the length of the extended barrel cylinder. The barrel cryostat is supported by four plates which are bolted to the saddles and transfer the load of the cryostat
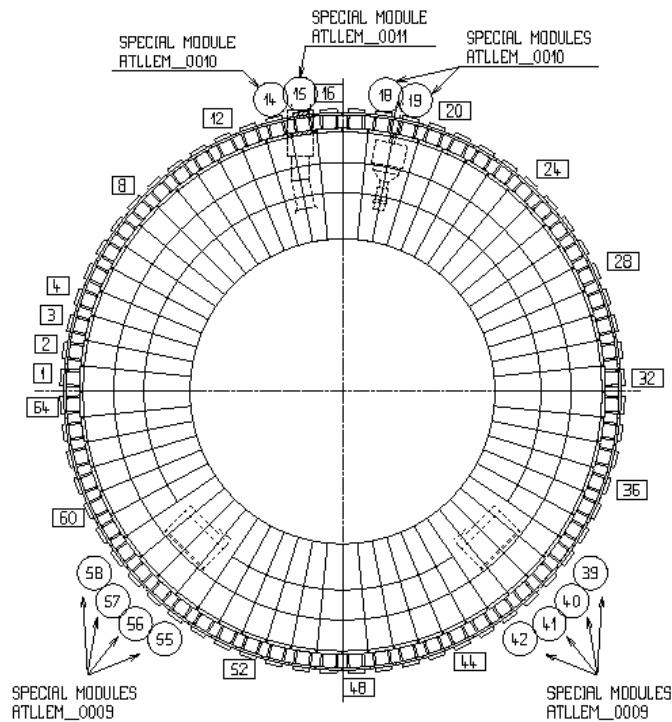
Figure 10: Location of special modules on the Extended Barrel calorimeter. Sides EBA and EBC are mirror symmetric about the interaction except for modules in position 14 and 15 and 18 and 19.

radially to the ATLAS main rails. To minimize the thickness of these plates while insuring sufficient resistance to buckling, the plates are bolted to the calorimeter structure using high strength rods which pass through the calorimeter, replacing source tubes in these locations.

Figure 12 shows two structures used to support the end cap cryostat and illustrates the four key features of the design. This comprises a stiffening gusset, the saddle plate with threaded holes for swivel bolts and clearance holes to access the module connecting plate bolts (which is identical for barrel end extended barrel saddles) and the back cryostat support plate which carries the majority of the weight of the end cap calorimeters and transfers it directly to the ATLAS main rails. To avoid any additional dead material, such as would result from a similar plate, the support on the inward (towards the IP) side of the end cap is special in that in this case the cryostat feet sit on jacks located at the inner radius of the tile calorimeter (and its mirror image). To provide space for these support jacks, the first three submodules are cut to the necessary geometry and steel plates welded across the cut master plates. The geometry of this support is shown in figure 12, which also shows the layout of hydraulic jacks used for the final positioning of the cryostat. This will be difficult region for energy measurement due to both the material of the support and the compromised response of the tiles in the cut submodules.

Many man years of engineering analysis was carried out to insure the adequacy of the tile calorimeter structural design [8–15] and were the subject of intensive engineering review. However, the details of these calculations are beyond the scope this paper. Globally, Eurocode was employed and where possible, analytical calculations were compared to those obtained by finite element modeling. In general 2-dimensional finite element models were used, however, in some critical regions, such as the saddles and cryostat supports, 3-dimensional models were also constructed (and cross-checked against the 2-dimensional models). Based on these calculations, for the most sensitive connections, (for example welding of the inner radius plate) technician certification and 100% non-destructive inspection was em-
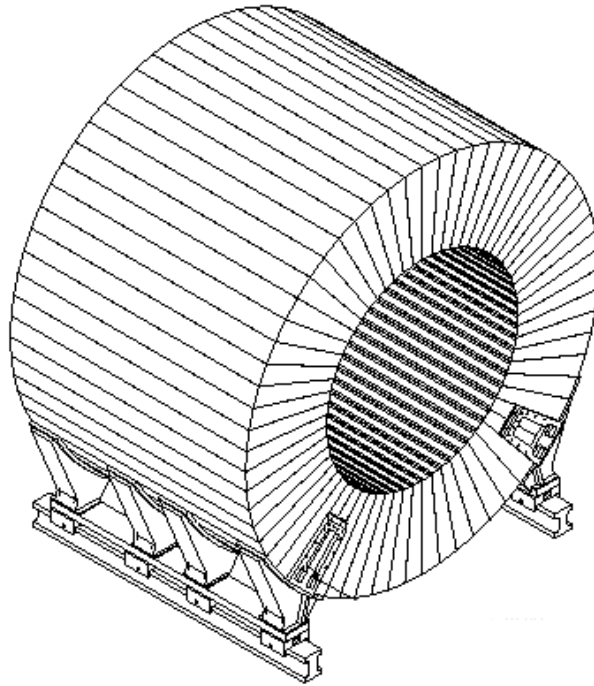
11

Figure 11: Schematic of the support saddle used to transfer the weight of the tile calorimeter to the ATLAS main rail systems. A mirror symmetric saddle supports the cylinder on the opposite rail.
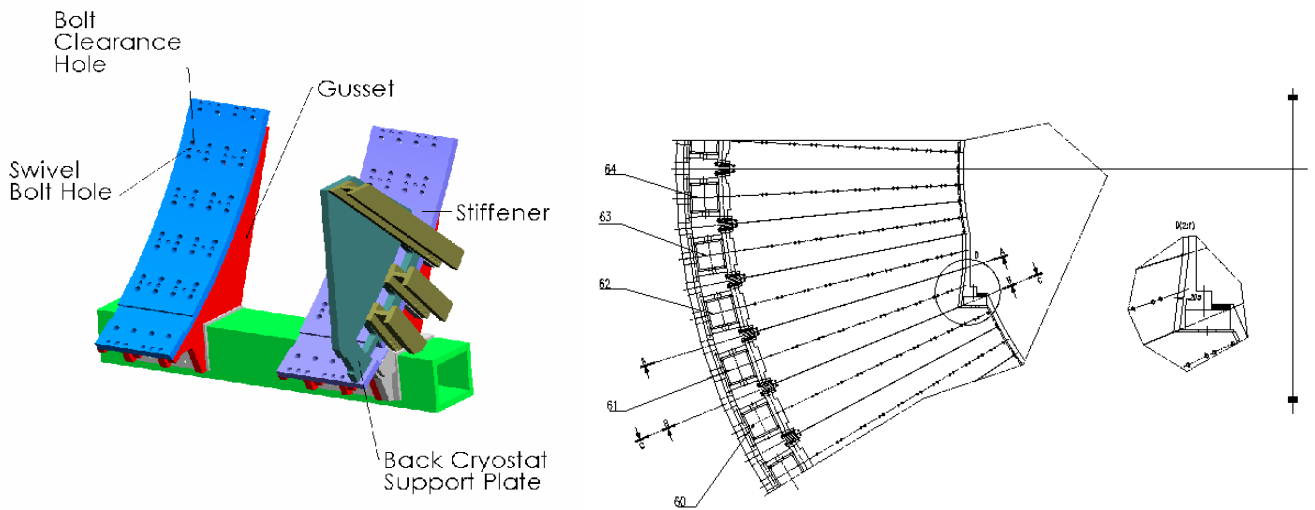

Figure 12: Schematic of one of the pairs of saddles used to support the extended barrel calorimeter (left). The geometry of the inner support of the end cap cryostat (right).

ployed during construction. Destructive testing of test pieces was used where engineering criteria did not fall into a standard protocol [16–18]. One such test was of the bolted connection between the submodule and the support girder, and was used to determine the maximum allowed stress both in the mounting bolts and in the threads cut in the girder steel. This test was also used to establish an empirical measure of the rigidity of the submodule and its connection to the girder for use in subsequent finite element analysis of the calorimeter structure as a whole.

The loading conditions in this design vary throughout the stucture and an example of this is shown in figure 13 which shows the forces at the front face of the calorimeter as a function of the position of the module and of the number of modules in the assembled cylinder. It also shows that at the top of the cylinder (module 32) the load at this interface is zero. These forces were used to determine the minimum area required for the shims at the inner radius of the structure. The forces at the outer radius of the calorimeter (the link plates) show even greater variation. Above the saddles the force is in compression, while the lower section
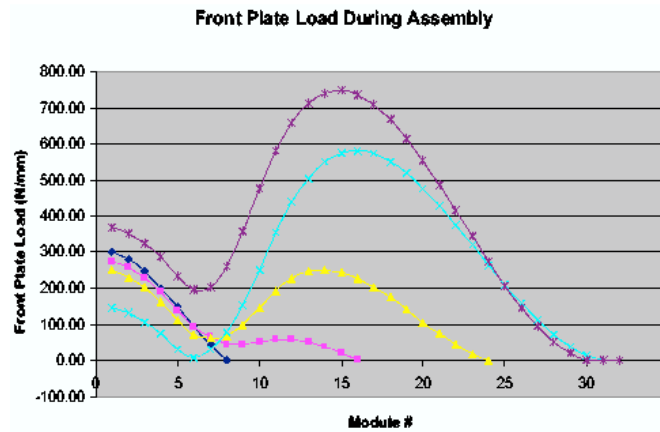

Figure 13: Calculated force at the inner surface of the module-to-module interface as a function of module position in the calorimeter and as a function of the number of modules assembled. Module 0 is located at the bottom of the cylinder and module 32 is located at the top of the cylinder.

between the saddles is in tension (i.e. the modules want to pull apart). In this case the calculations were used to establish the number and diameter of pins needed to carry this shear force.

Seismic forces were evaluated using the methodology given in Eurocode and an assumed acceleration of 0.15g. Blocks between the saddles and the calorimeters prevent any relative movement along the beam line in this situation. An additional consideration which results is non-static forces arises during installation when the barrel cylinder is moved from its assembly location below the cavern access shaft to the interaction point (a distance of about 12 m), or during routine movements of the two extended barrel calorimeter for detector maintenance. Guide brackets, attached to the saddles, have been designed to accommodate the maximum non-uniform loading, which would occur if one of the hydraulic cylinder were to fail and the calorimeter moved using only a single cylinder from one rail.

3   Submodule Construction

As was discussed above, the calorimeter design involves only a small number of basic components. The assembly begins with the rolling and cutting of steel sheets, 5 mm thick for master plates and 4 mm thick for spacer plates with a thickness specification of ±0.05 mm and ±0.04 mm respectively [3] [4]. To achieve the specification of +0/-0.1 mm on the outer envelope of the master plate, as demanded by the specification for the design gap between modules, a precision die was used for their fabrication [4] [5]. As the stamping die could produce the full plate geometry in a single pass (holes, keys and envelope), this proved to be an extremely cost-effective manufacturing approach. Die stamping was also used to produce the spacer plates, again to realize the specification on envelope and for cost-effective production [6]. All remaining basic elements were either simple procurements or fabricated at the collaborating institutions.

Submodules were constructed at 9 institutions. The basic absorber unit of the calorimeter structure is formed by the lamination of two master plates and two (half) sets of spacer plates as shown in figure 14,
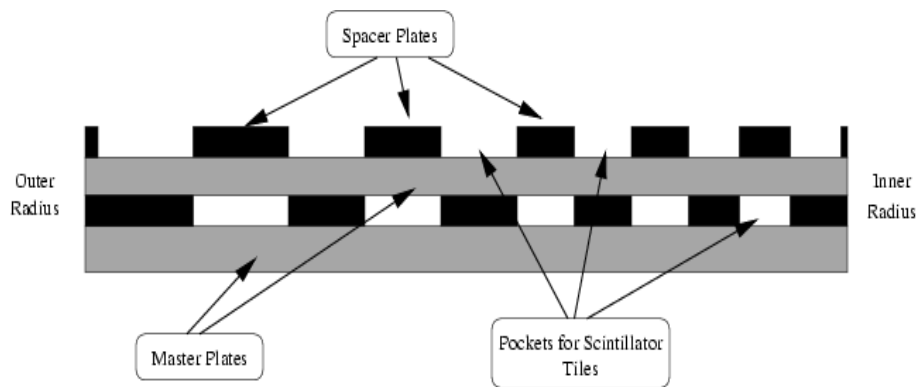
Figure 14: Schematic of the basic unit of the calorimeter absorber structure: the full period. This comprises two master plates and two alternating sets of spacer plates stack such that the voids between master plates form the slots into which the scintillator tiles are to be inserted.

where one can also see the progressive increase in the length of the spacer plates as one moves toward the outer radius of the structure (done to reduce the piece-count and thereby the overall handling costs.) A submodule is built up by alternating a master plate with layers of spacer plates which were glued and
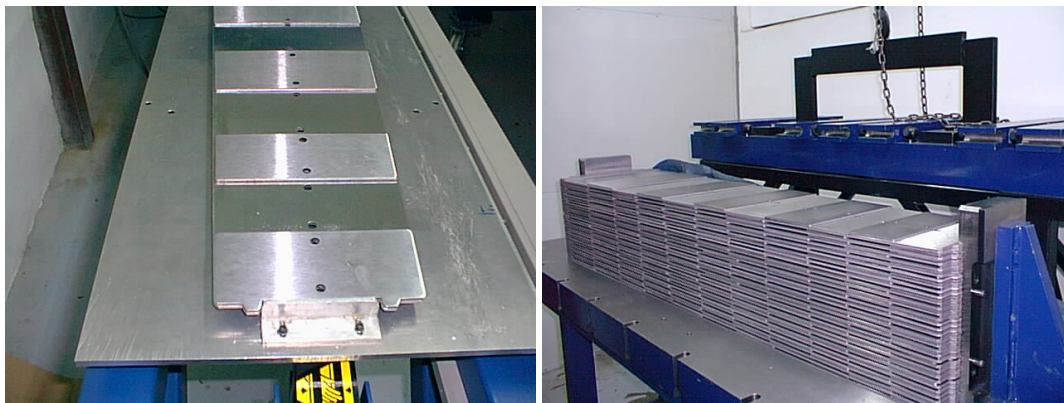

Figure 15: One layer of spacer plates being fastened to the master below through spring pins and structural adhesive (left). A submodule being assembled on the stacking fixture, the keys at either end precisely align the master plates (right).

pinned as shown in figure 15 (left). The role of the glue is crucial in the design providing mechanical strength and compensation for the tolerances of the 64 plates stacked for a basic submodule. The position of the glue deposition and volume of glue was carefully controlled to give a glue line of sufficient shear strength. This deposition was done by a variety of ways ranging from a semi-automatic gluing machine to manual deposition using a glue gun and template. The mechanical connection via steel spring pins insures the geometrical positioning of the spacer plates relative to the master plates. The tubes used for cesium calibration system pass through these spring pins, which therefore align the cesium capsule to the scintillator tiles. To insure their overall geometrical and structural uniformity, a standardized stacking fixture was used to construct submodules. This fixture is shown in figure 15(right). It is comprised of thick steel bottom and top plates together with precision aligned keys into which the matching keyways on the master plates could be engaged. A finished submodule is shown in figure 16 below, where the slots in which the scintillators will be inserted are clearly visible. A mounting bar, one of two which are welded to the master plates once the glue has cured is seen at the outer radius of the submodule (leftmost area of figure 16).

14

Submodule construction included a detailed quality control plan which was also developed as part of the design to insure uniform production throughout the nine submodule construction sites. The QC protocol included careful tracking of glue deposition quantities and curing time, inspection of the welding of the

Figure 16: A finished standard submodule.

mounting bars, and a series of measurements of module flatness, stack height and envelope. The key dimensional control was on the height of the submodule stack as good maintenance of this height was essential to insure that all submodules could be successfully mounted on the module support girder. A representative example of the submodule stack height for the submodules constructed at one of the construction sites is shown in figure 17. In general, the submodule followed a football shape as a result of weld shrinkage such that near the inner radius the weld caused the submodule to be lower than nominal and higher than nominal near the center of the submodule. However, as is seen in figure 17, this effect was quite reproducible and largely within the height specification of +0.3mm and -1.5mm relative to nominal. The distribution of the maximum stack height deviation from nominal for all submodules
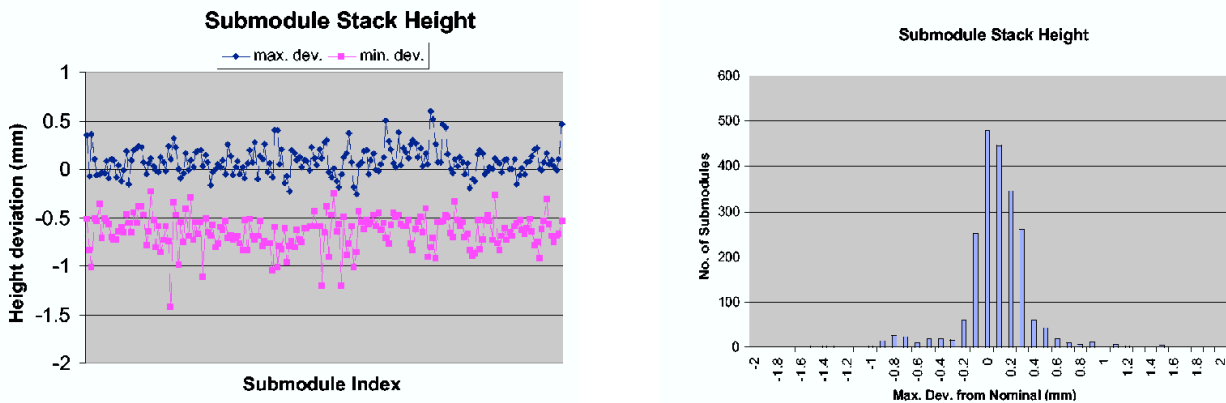

Figure 17: Stack height monitor data for a typical submodule production series at one of the submodule construction sites (left). Maximum deviation from nominal for all submodule constructed for use in the ATLAS TileCal (right).

constructed is shown in figure 17. The vast majority of submodules fall within the required envelope. The small number of submodules, whose height exceeded 0.6mm from nominal were identified with pallets of raw sheets whose thickness exceeded the design thickness specification. A small number of custom submodules with heights of -1.00 to -1.5mm relative to the nominal height were constructed and mounted adjacent to these higher submodules during module construction.

Submodule construction concluded with the application of a thin layer of protective paint and a subsequent final QC check to insure that paint build-up in the slots would not impede insertion of scintillator tiles or the fibre channels. More details on submodule construction and quality control can be found in references [7] [19].

15

4 Module Production

Module construction was carried out at three collaborating institutions, where appropriate facilities for handling and storage were available. Each of these institutions was assigned the task of construction of one of the major sections of the full calorimeter: Barrel (LB), Extended Barrel C (EBC), and Extended Barrel A (EBA). Other than its physical size, the tile calorimeter module is a simple object. Three components form the basic absorber structure: the structural support girder, front plate and submodules. In addition, external endplates are used to provide for mounting of services on the end surface of the calorimeter and so-called 'girder rings' are inserted to support the readout electronics and position the fiber bundle. Finally, precision reference marks (fiducial marks) are attached to the ends of the module for use in calorimeter assembly.

There are two critical constraints pertaining to module assembly: the overall module envelope which was required to lie within +0.5 mm of the nominal envelope, and the girder ring positioning such that the electronics drawer alignment to them was precisely maintained while still allowing the drawer freedom to move in and out of the girder volume. Tooling was developed to insure that these constraints would be met and the overall construction approach closely followed that which was developed in the prototype phase of the project and which is described in the Tile Calorimeter TDR [2]. Further details on the use of this tooling can be found in [7] [20] [22].

Figure 18: The assembly base used for extended barrel module construction (left). The module alignment system, used at one of the extended barrel module assembly sites. It couples the alignment of the girder via survey pins to the plate inserted at the inner radius of the module and a survey mark and plumb-line on a fixed support placed behind the module (right).

4.1 Module Assembly

Module assembly followed the same sequence at all three locations. First, the support girder is leveled and bolted to a module assembly base as shown in figure 18. A right angle, or precision level, is then used to align submodules vertically on the girder. Shims at the bolted interface insure that the girder

key is never in contact with the submodule and also correct the submodule position, bringing it inside the overall module envelope. The alignment of submodules at the inner radius was accomplished by different techniques at the different locations. In the case of the barrel assembly, a laser was used with the fixed endplates at either end of the assembly base establishing the alignment reference system, as shown in figure 19. In the case of the extended barrel modules, which are half the length of the barrel module, a somewhat simpler approach was used. In one case a precision electronic level was used to align vertically the center of the submodule, as defined by the holes for the source tubes. In the second case, an alignment fixture was placed in the inner radius key of the submodule and an optical transit used to set the submodule vertical and centered on the centerline of the girder (as established by a reference hole placed in the girder during fabrication.)
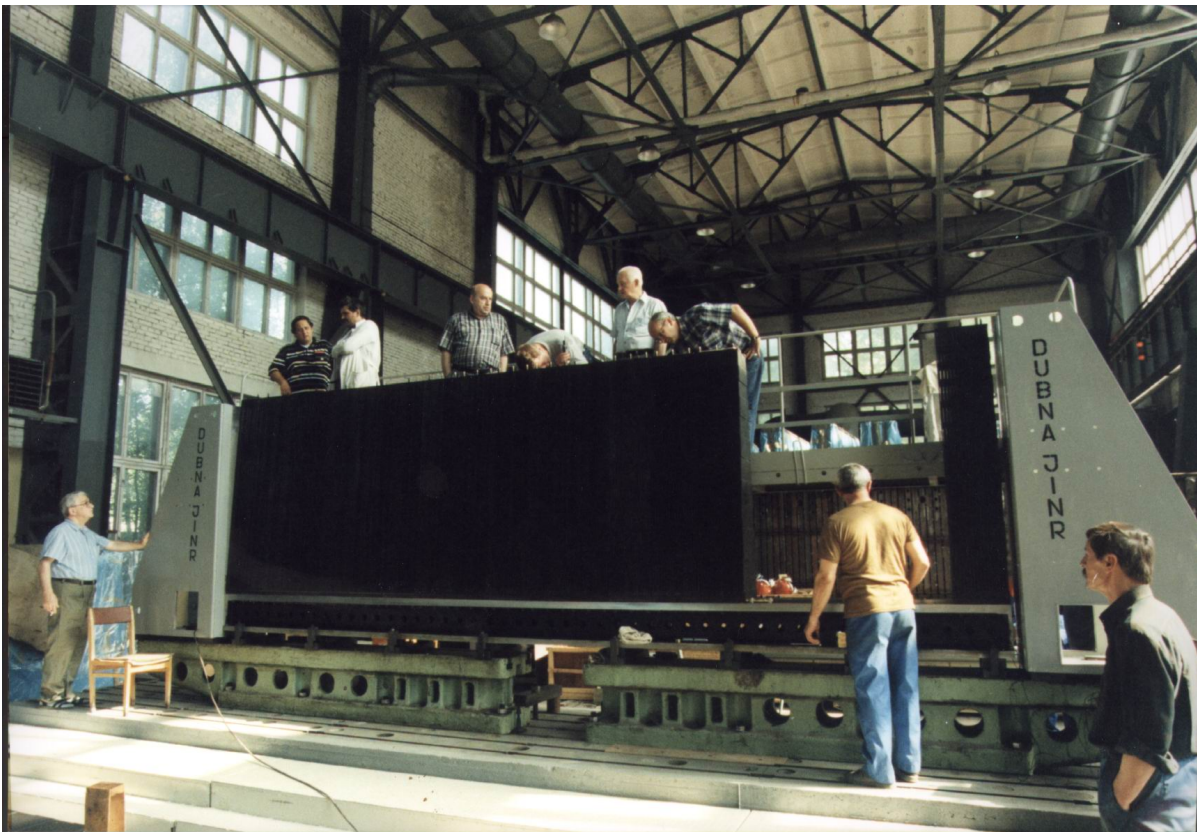

Figure 19: Barrel module assembly. The endplates are aligned to the assembly base to establish the vertical alignment of modules, as well as to establish the centerline of the girder and inner radius of submodules.

Mounting endplates at the end of the module was similar to mounting submodules, except that these plates are undercut by 0.5mm relative to the module envelope and therefore great precision is not required for this operation. Following a basic envelope check, the inner radius plate was welded into the inner key, joining together all submodules as well as the endplate.

Quality control protocols were developed during the prototype development and used during module construction. These included two important checks on the mechanical integrity of the module:

A cross check of the preload on submodule mounting bolts, which is a particular concern in the extended barrel assembly where different preloads are used in different regions of the calorimeter (i.e. for different modules and for different submodules on a module.)

17

100% non-destructive inspection of the weld of the front plate (to insure continuity of the bearing surface at the inner radius in the final assembly)

In addition, an extensive set of measurements was made of the geometrical envelope. For the barrel these again made use of the laser system used during module assembly [20]. In the case of the extended barrel modules a 2m precision straight edge was used in conjunction with feeler gauges to measure the out-of-plane deviation of absorber plates along the length of the module. The deviations along the length of the module, or from outer to inner radius, reflected the different types of systematic bias associated with the different approaches used for submodule mounting. However, the only important parameter is the maximum deviation from nominal, which was less than 0.5mm for all points measured on all modules. After instrumentation the module surfaces were covered by a sheet of black tedlar and aluminum tape used to cover mounting holes inside the girder to provide light sealing. During calorimeter final assembly as a further precaution, a bead of RTV was placed at the outer edges all round the module.
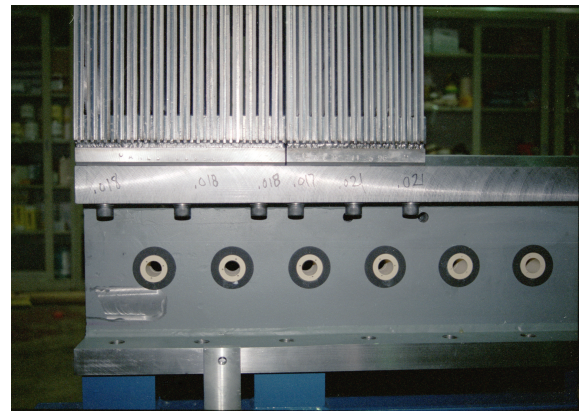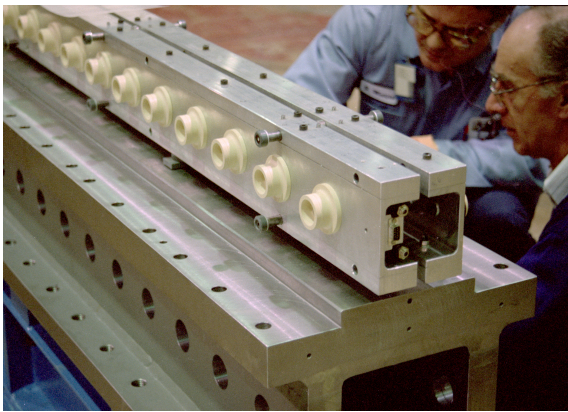
4.2 Girder Ring Insertion

Figure 20: The pneumatic tool used to insert and locate the inner pieces of girder rings for gluing resting on top of a girder ready to have girder rings installed (left). The outer girder rings following gluing, the black rings are the foam rings used to seal the plastic inserts to the girder surface (right).

An ingenious approach was developed to decouple the very high precision needed for the interface to bring calorimeter light signals to the photomultiplier tubes from the precision required to position the holes in the girder through which the fibres enter. Figure 20 (left) shows a close-up of the penetrations in the girder. They are large holes in the structure and if the position to the tolerance required by the optical light coupling to the photomultiplier tube, then the cost of their fabrication would have been prohibitive. Instead of this the approach used was to glue plastic transition pieces termed 'girder rings' into these holes. The tool shown in figure 20 (left) was used to position and precisely locate the inner section of the girder rings. The electronics drawer rides on, and is located relative to these rings (as seen in figure 5) such that the optical coupling is geometrically controlled to a precision of 0.3mm. The outer sections of the rings mate with the inner sections and the full assembly is glued into the girder with foam seals at inner and outer surfaces insuring minimal leakage of glue onto the girder surfaces. The girder rings themselves are the element which establishes the optical alignment path for fibres during instrumentation.

18

4.3 Mounting of Fiducial Marks

The final task associated with module assembly was to attach reference marks to the module endplates and fingers, for use during cylinder assembly. These reference marks are in fact small fixtures, which can accept different types of inserts and survey pins to allow either optical or physical measurements of the position to be made . In addition, to standard targets for optical surveying and photogrammerty, a custom tool was constructed to use the hole in which these devices are inserted as a locating point for a precision ruler in order to make rapid measurements of the distances between modules. Custom tooling is used to position these fixtures (termed fiducial marks below) at three radial locations (close to the inner and out radii of the module, and at a location roughly in the middle of a module radially at a location which is not obscured by the flanges of the cryostats). The tooling establishes the reference for these fiducial marks from the z position of the end of the support girder, and establishes the centre line for fiducial mark installation using a precision level and the outer edges of the girder bearing surfaces (figure 21). The typical

Figure 21: Mounting fiducial marks on the endplates of completed modules for use in surveying module positions during final assembly

precision is 0.3 mm in all three coordinates. More details of this part of the module assembly can be found in reference [20].

5 Calorimeter Installation

The calorimeter is designed as a self-supporting cylinder formed by the modules which bear on each other at the inner and outer radii. The calorimeter is supported on simple supports by the saddles and as a result of this support, the module interfaces are in tension below the saddles and are in compression above the saddles. Moreover the position of the support has been chosen such that the system is stable once 18 modules have been mounted (i.e. just at the top of the saddles) and no load is carried across the two modules at the top of the cylinder.

As the system is initially unstable, the calorimeter assembly was carried out initially on an external support frame until the point at which the support saddles were mounted and the load transferred to them (at 18 modules, which is the minimum required for stability). Of essential importance at this stage in the assembly is the insertion of the shear pins which take the tension load below the saddles. These pins are 33 mm in diameter, are 80 mm in length and must be match-drilled through the girder link plates into the girder top plate. Although, the link plates and girder included pre-drilled holes with undersized diameter, this task required no small amount of ingenuity and machinist skill. In some locations, due to insufficient space to mount a commercial magnetic-base drill, a custom drill was designed and fabricated. The assembly fixture was also designed to serve also as a fixture on which a pre-assembled section of calorimeter could be lowered into the ATLAS cavern. In the case of the barrel cylinder, this comprised 8 modules, and for the extended barrel cylinders this comprised 18 modules as well as the support saddles. Therefore, the critical and time-consuming task of inserting the shear pins was carried out on the surface and with relatively convenient access to the calorimeter structure. In addition to the benefit

in the reduction in installation time in the cavern, this also implied that the geometry realised during the final assembly would closely follow that of the surface assemblies. Finally, in the case of the extended barrel cylinders, due to the geometry of the inner support, the cryostat must be installed once 24 modules are mounted, whereas in the case of the barrel cylinder the barrel cryostat was installed once 32 modules were mounted, but the load not transferred to its supports until completion of the TileCal cylinder.
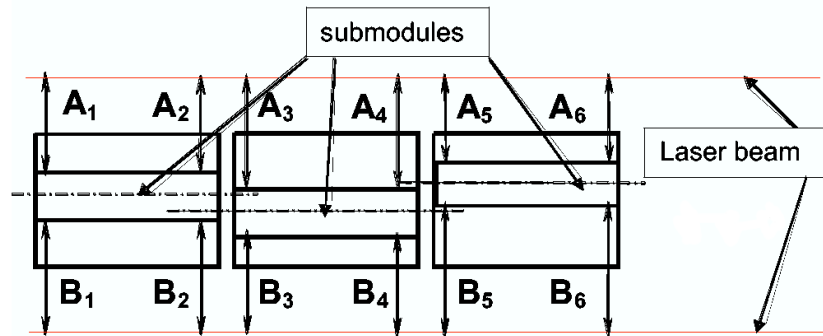
Figure 22: A schematic of the module envelope variation showing the laser-based scheme for measuring the module envelope along its full length.

The Tile calorimeter is geometrically constrained by the stay clear envelope of the barrel and end cap cryostats as well as the inner chambers of the muon system. The global envelope was set at +5 mm outward and -10mm radially inward. A key point to appreciate is that although the basic manufacturing tolerances were at the level of 0.2mm - 0.4mm, these tolerances themselves are not sufficient to permit the cylinder to achieve the radial envelope specification while maintaining a uniform module-to-module gap of 1.5mm. In addition, the bearing condition at the inner radius was changed from that assumed in the TDR design where we assumed that the load transfer at the inner radius is transferred through shims between the inner radius weld bars. Instead, for the final design we adopted a solution in which the bearing load is transferred through shims between the submodule surfaces in the first 2cm from the inner radius. This solution was necessary to accommodate the bearing forces in the region of the inner cryostat support of the extended barrel, and we decided to adopt it uniformly for the entire calorimeter. There are two consequences to this choice, which had a fundamental effect on the assembly:

1 The shim thickness must be determined for each submodule position along the girder

2 The setback of the spacer plates relative to the master plates in the submodule results in a scalloped interface and the shims deform under load

The scheme used to determine the nominal shim thickness as a function of shim position is shown in figure 22 [20]. A laser beam is referenced to the module endplates, which themselves are referenced to base and center of the support girder during module construction. A quadrant-style photodetector is illuminated by the laser beam, and the relative position of the beam to nominal is determined by centering the response of the four quadrants of the detector using a simple bridge circuit. The detector is scanned along the bearing surface of the girder and along the module at the radius at which the inner radius shims are glued. The data are recorded and used to determine the shim thicknesses to be used for the interface between each module pair. This is the so-called nominal shim thickness.

Due to the self-supporting feature of the design of the tile calorimeter, and the size of the structure, the assembly of the calorimeter cylinders began with a surface assembly to establish the validity of our
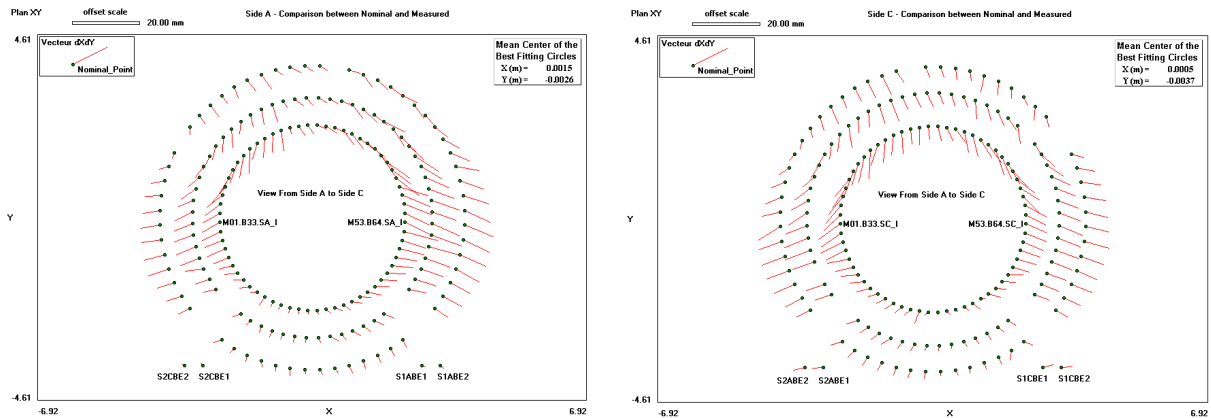
Figure 23: Deviation from the best fit center for fiducial mark positions on both sides of the barrel cylinder following the completion of the surface assembly. The three sets of points are for the fiducial marks at the inner,. middle and outer radius of the module as discussed above.

assembly concepts prior to installation in the cavern [21]. Several measurement techniques were used to monitor the preassembly, all of which used the fiducial marks described above as the reference points. The techniques comprised: a custom precision ruler used to measure the chord length between opposite modules; optical survey of the positions of the fiducial marks, caliper measurements between fiducial marks on adjacent modules. Following disassembly of the structure, shims were removed and measured by micrometer. Several key observations were made during the surface assemblies:

. The precision required for the shim thickness is of order 50 microns

. Shim deformation at the inner radius is large and dependent on the module position

. Shim deformation is dependent on the exact load conditions (e.g. number of modules in the assembly, before or after loading of the cryostat in the case of the extended barrel cylinder)

. Due to the changes in shim thickness as they deform, the cylinder shape also changes dramatically as a function of the load conditions.

. Due to the lever arm of the cylinder, small changes in the gap between modules at the inner radius have a large effect on the geometry of the cylinder (and in particular on the adjustments needed to insure that the cylinder is closed).

A full surface assembly was completed for the barrel (excluding the load of the barrel cryostat). In the case of the two extended barrel cylinders a full surface assembly of one was completed (also excluding the load of the endcap cryostat load), while for the second extended barrel, the surface assembly was carried out up to the point at which a load equivalent to that of the endcap cryostat could be installed (and the system remain gravitationally stable). A summary of the survey results for the surface assembly of the barrel cylinder are shown in figure 23. The cylinder is slightly flattened, somewhat more at the top than at the bottom, and has bulged outward at the sides. The maximum outward deviation is approximately 5.5 mm and the maximum inward deviation is approximately -4.5 mm. Therefore the cylinder is almost entirely within its design envelope. Both sides of the cylinder are essentially identical in shape indicating that no twisting occurred during the assembly process.

The data taken during the surface assembly of the cylinders were used to validate and establish the parameters used in two independent numerical models which were subsequently used to monitor the cylinder geometries during final calorimeter assembly in the ATLAS cavern (primarily shim thickness

21

and deformation as a function of shim location). These models were an essential part of the scheme by which the hermeticity of the calorimeter cylinders was achieved. They were used to correct for the expectedly large deformation in shims when determining the nominal thicknesses, to compensate for the additional shim deformation resulting from the cryostat loading, to correct for errors made during the surface assemblies and to determine shim corrections as needed during the final stages of the calorimeter assembly. Whereas during the surface assembly of one extended barrel the final module was out of position radially by approximately 40mm, with a gap for its insertion too small by about 10mm, during the final assembly the gap for insertion of the final module was essentially nominal and the cylinder fell with its design envelope. For the extended barrel cylinders, a partial assembly comprising of 18 modules (and saddles) on the assembly frame was the initial unit lowered into the ATLAS cavern. In the case of the barrel cylinder this unit was 8 modules. Following surface assembly these sections of the cylinder were never disassembled.

Figure 24: Installation of the barrel cryostat in the ATLAS cavern (left). The installation of the final TileCal module in the EBC cylinder (right).

The final assembly in the cavern benefited enormously from the surface assembly experience. The tooling designed and constructed to manipulate modules into the required orientation for mounting was fully qualified, the necessary expertise acquired in module handling and preparation, and techniques (including numerical modeling) developed for geometrical control. Figure 24 shows two of the key steps in the final assembly; installation of the barrel cryostat, and the insertion of the last module (in one of the extended barrel modules) where one can obtain some sense of the gap into which this module was inserted. This figure also vividly illustrates an important feature of the engineering design: namely that that the stability of the cylinder does not require any forces to be restrained at the top of the cylinder. It is also important to note that opening the cylinder to provide space for the insertion of the last module was considered to be undesirable. Although mechanically realisable for the barrel, the result would be to push the sides of the cylinder outside their allowed envelope. In the case of the extended barrel calorimeter, this option is not even mechanically possible due to the effect of the load from the end cap cryostat. The calculations and measurement made during module installation, together with shim adjustments, allowed control of the gap for the final module to within 0.5 mm.

The final assembly task comprised a full survey of those fiducial marks which still remained visible once the cryostats were installed. Optical and photographic survey methods were used and results compared to those obtained by the precision ruler, where available. The summary of these results for the barrel cylinder is shown in figure 25, which shows the measured positions relative to the nominal position (i.e. the beam center). The shape of the cylinder is essentially the same as was obtained during the surface assembly. Similar results were obtained for both extended barrel calorimeters. A full compi-
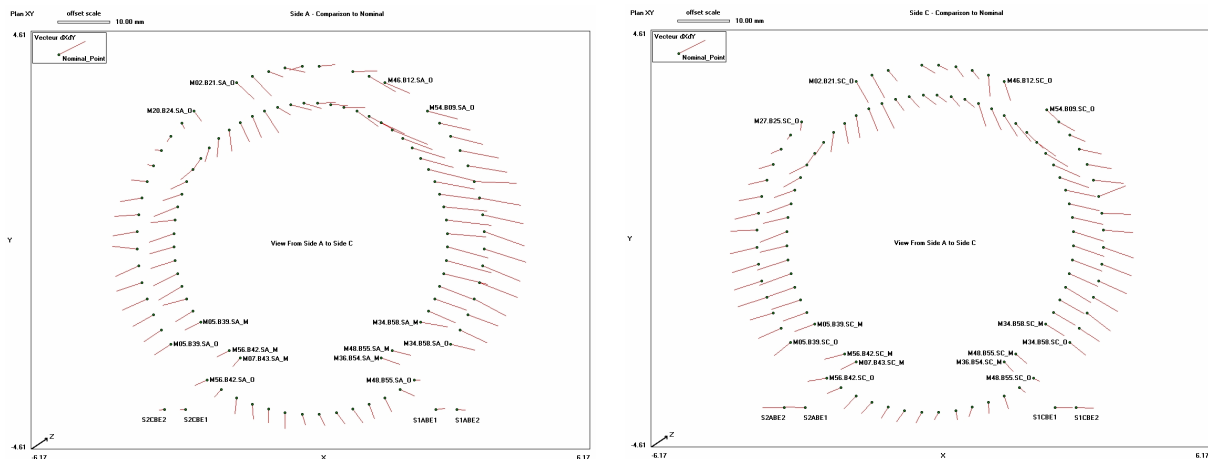
Figure 25: Deviation from nominal for fiducial mark positions surveyed for following the completion of the final assembly of the barrel cylinder in the ATLAS cavern.

lation of these results is available in the EDMS database [23]. With some small variances, the envelopes
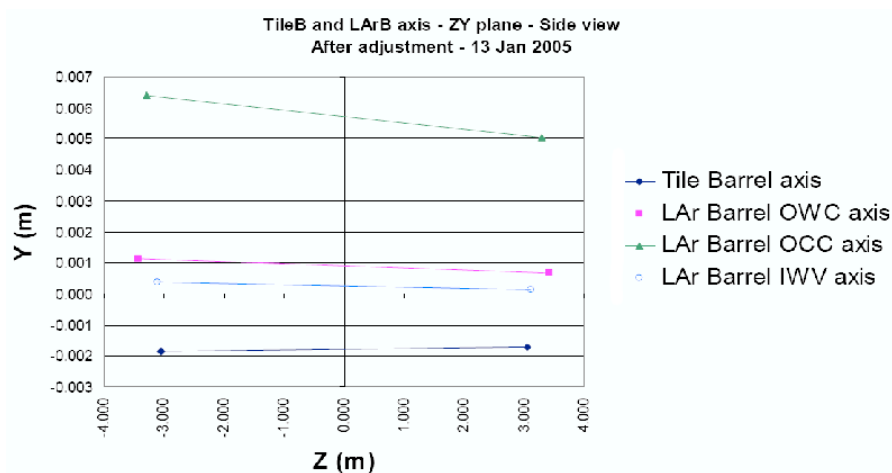

Figure 26: Height (y) of the nominal centre for the tile calorimeter and barrel electromagnetic calorimeter as a function of position along the beamline (z).

for all three cylinders fall within the design radial envelope of +5 mm and -10 mm relative to the best bit centre. This centre is typically low by about -2 mm relative to nominal in the case of the barrel and varies with location for the extended barrel cylinders due to the asymmetric loading of the end cap cryostat. These height deviations can be compensated using hydraulic jacks on which the calorimeters are supported. However, this compensation must also take account of the detectors which are support on the tile calorimeter and have their own as-built deviations from nominal. This is a particular issue for the barrel calorimeter as it supports both the barrel cryostat, which itself supports the ATLAS inner tracker. Once installed, the only vertical adjustment is provided by the jacks supporting the tile calorimeter. The installed position of the electromagnetic calorimeter was chosen to have highest priority. The resulting positions of the tile calorimeter and cryostat are shown in figure 26, where the maximum vertical deviation from the beam line is 2 mm. Transverse to the beam line the cylinders are on axis within the precision of 1 mm provided by the calorimeter guide brackets.

In conclusion, following an odyssey of over 10 years the ATLAS scintillating tile calorimeter was

designed, constructed and installed to specification in the ATLAS cavern where it is now being commissioned and readied for first physics data-taking in 2008.

6   Acknowledgements

References

[1] ATLAS Collaboration, Detector amd Physics Performance Technical Design Report CERN/LHCC/99-14/15 (1999)

[2] ATLAS Collaboration, Tile Calorimeter Technical Design Report, CERN/LHCC/96-042 (1996)

[3] T. Davidek et al., Steel absorbers for the Hadronic Tile Calorimeter of the ATLAS Experiment, ATL-TILECAL-99-008

[4] N. Hill et al., Plate Stamping of Master Plates for the Tile-Cal Hadronic Calorimeter used in the ATLAS Detector at CERN, ANL-HEP-TR-96-42

[5] J. Proudfoot et al., Master plate production for the Tile Calorimeter Extended Barrel Modules, ANL-HEP-TR-99-04

[6] B.A. Alikov et al., ATLAS Barrel Hadron Calorimeter General Manufacturing Concepts for 300000 Absorber Plates Mass Production, JINR E13-98-135

[7] V. Yu Batusov et al., ATLAS Hadron Tile Calorimeter: Experience in Prototype Construction and Module Mass Production, Physics of Particle and Nuclei, Vol 27 No 5 (2006)

[8] V. Guarino, Steel Specification for the ATLAS Tile Calorimeter ANL-HEP-TR-98-12

[9] V. Guarino, Quality assurance plan for the ATLAS raw steel sheets ANL-HEP-TR-98-11

[10] V. Guarino, Stress analysis of the welds in the girder ANL-HEP-TR-98-06

[11] V. Guarino, Analysis of Barrel Support Saddles and Forces between Modules during Assembly ANL-HEP-TR-07-10

[12] V. Guarino, J. Grudzinski, E. Petereit, Extended barrel Support Saddle Design and Analysis ANL-HEP-TR-01-097

[13] V. Guarino, Analysis of the Connections between Modules in the EB ANL-HEP-TR-02-056

[14] V. Guarino, Analysis of EB Support Saddles and Forces between Modules during Assembly ANL-HEP-TR-02-058

[15] V. Guarino, Stability of EB when the Cryostat Load is Applied ANL-HEP-TR-04-65

[16] Blocki, J; Guarino, V; Miralles, Ll; Topilin, N D, STUDY, EVALUATION AND TEST OF SUB-MODULE TO GIRDER BOLTED JOINT, ATL-TILECAL-2000-007

[17] Blocki, J; Brunel, B; Nessi, M,Testing of welds in the submodule, ATL-TILECAL-98-136

[18] Blocki, J; Brunel, B; Hill, N; Nessi, M; Proudfoot, J; Rose-D, Mechanical Tests for Sub-module, ATL-TILECAL-97-110

[19] L. Kocenko et al., Production summary for Submodule fabrication at Argonne for the ATLAS Tile Calorimeter, ANL-HEP-TR-07-69

[20] V. Yu Batoussov et al., Development and application of high precision metrology for the ATLAS Tile Calorimeter Construction, JINR E13-2004-177

[21] V. Batusov et al., Development and application of high precision metrology for the ATLAS Tile Calorimeter Construction (the Pre-assembly experience and lessons), JINR E13-2005-42

[22] V. Guarino et al., Production summary for Extended Barrel Module fabrication at Argonne for the ATLAS Tile Calorimeter, ANL-HEP-TR-07-68

[23] https://edms.cern.ch/nav/ATL-0000007367